

Gamma irradiated nanostructured NiFe₂O₄: Effect of γ -photon on morphological, structural, optical and magnetic properties

Sapan Kumar Sen^{a,*}, Majibul Haque Babu^b, Tapash Chandra Paul^c, Md. Sazzad Hossain^d, Mongur Hossain^e, Supria Dutta^f, M. R. Hasan^g, M. N. Hossain^h, M. A. Matin^h, M. A. Hakim^h, Parimal Bala^c

^aInstitute of Electronics, Atomic Energy Research Establishment, Bangladesh Atomic Energy Commission, Dhaka-1349, Bangladesh

^bBasic Science Division, World University of Bangladesh, Dhaka-1205, Bangladesh.

^cDepartment of Physics, Jagannath University, Dhaka-1100, Bangladesh.

^dDepartment of Physics, University of Dhaka, Dhaka-1000, Bangladesh.

^eHunan Key Laboratory of Two-Dimensional Materials, State Key Laboratory for Chemo/Biosensing and Chemometrics, College of Chemistry and Chemical Engineering, Hunan University, Changsha, 410082 China.

^fMinistry of Education, Government of the People's Republic of Bangladesh, Dhaka, Bangladesh.

^gMaterials Science Division, Atomic Energy Center, Dhaka, Bangladesh Atomic Energy Commission, Dhaka-1000, Bangladesh.

^hDepartment of Glass & Ceramic Engineering, Bangladesh University of Engineering & Technology, Dhaka-1000, Bangladesh.

Abstract

The current manuscript highlights the preparation of NiFe₂O₄ nanoparticles by adopting sol-gel auto combustion route. The prime focus of this study is to investigate the impact of γ -irradiation on the microstructural, morphological, functional, optical and magnetic characteristics. The resulted NiFe₂O₄ products have been characterized employing numerous instrumental equipments such as FESEM, XRD, UV–visible spectroscopy, FTIR and PPMS for a variety of γ -ray doses (0 kGy, 25 kGy and 100 kGy). FESEM micrographs illustrate the aggregation of ferrite nanoparticles in pristine NiFe₂O₄ product having an average particle size of 168 nm and the surface morphology is altered after exposure to γ -irradiation. XRD spectra have been analyzed employing Rietveld method and the results of the XRD investigation reveal the desired phases (cubic spinel phases) of NiFe₂O₄ with observing other transitional phases. Several microstructural parameters such as bond length, bond angle, hopping length etc. have been determined from the analysis of Rietveld method. This study reports that the γ -irradiations demonstrate a great influence on optical bandgap energy and it varies from 1.80 and 1.89 eV evaluated via K-M function. FTIR measurement depicts a proof for the persistence of Ni-O and Fe-O stretching vibrations within the respective products and thus indicating the successful development of NiFe₂O₄. The saturation magnetization (M_S) of pristine Ni ferrite product is noticed to be 28.08 emu/g. A considerable increase in M_S is observed in case of low γ -dose (25 kGy) and a decrement nature is disclosed after the result of high dose of γ -irradiation (100kGy).

Keywords: Sol-gel auto combustion; NiFe₂O₄; Gamma-irradiation; Rietveld refinement; Saturation magnetization; Optical bandgap

***Corresponding author:** sapansenphy181@gmail.com; ORCID ID: 0000-0001-5086-2758

1 Introduction

In recent years, nanocrystalline spinel ferrites have been investigated immensely owing to potential applications in chemical sensors, microwave absorbers, permanent magnets, high density recording systems, ferrofluid technology, biomedical, imaging and high-frequency device applications [1][2][3]. Importantly, they possess excellent both electrical and magnetic properties, which are extremely sensitive to the many factors such as chemical composition, synthesis method, annealing temperature or temperature treatment, and cation distribution at tetrahedral (A) and octahedral [B] sites [3]. Among the various spinel ferrites, however, NiFe₂O₄ (nickel ferrite) has drawn an optimum attention recently due to various applications in gas sensors [4], spintronics [5], microwave absorption [6], catalyst [7], lithium-ion batteries [8], hydrogen production [9], even in biomedicine [10] etc.. As more and more considerations have been devoted keenly to the nano-sized magnetic materials for inherent their unique properties compared to their bulk counterparts, so the scientific engrossment on nano-sized NiFe₂O₄ is on the expanding in the research community. In this direction, the magnetism of NiFe₂O₄ is predominantly intriguing due to its substantial saturation magnetization and unique magnetic structures. In general, NiFe₂O₄ belongs to an inverse spinel structure with Ni²⁺ ions on octahedral B sites (denoted as O_h-sites) and Fe³⁺ ions on both of the tetrahedral A (denoted as T_d-site and O_h-sites) sites equally [11]. This is typically maintained by the formation energy in favor of the reverse spinel rather than spinel structure [12]. It is also found to have the mixed spinel structure with the inverse one, i.e., some Ni²⁺ ions may occupy the T_d- site [11][13][14].

A general formula for a nickel ferrite structure is (Ni_{1-x}Fe_x) [Ni_xFe_{2-x}]O₄, where x is the degree of inversion. According to the crystal field theory (CFT), magnetic moments are rising from the local moments of the Ni²⁺ with 3d⁸ as well as Fe³⁺ with 3d⁵ electrons. Significantly, the net magnetization comes from the Ni²⁺ (O_h-sites) cations alone (~ 2μB), while Fe³⁺ moments (~ 5μB) in a high spin state for both O_h- and T_d-sites are antiparallel and abandon with each other [11]. However, the modification in physical properties (i.e structural and magnetic properties) of nanoferrites can be justified by instigating radiation damage by means of swift heavy ions[15], laser beam [16], proton [17] and gamma radiation [18]. Lately, several irradiation systems are implemented in the cutting-edge world because it is a striking tool for modifying the physical properties of nanoparticles in the research and development in commercial applications and industrial technologies like aeronautical and satellite communication, pollution control, material development, security systems and so on [15][19][20]. Upon electromagnetic nature, penetrating power, very short wavelength and all medium propagation property, the gamma ray (γ) is considered as ionizing radiation [21]. So, the present inquiry deals with an interaction of γ with NiFe₂O₄ which can tune its physical properties since it is known to generate controlled defects of

various types such as point, cluster, and columnar defects in the materials [22]. Besides, irradiation with γ rays contain the plausibility of dislocation of Fe^{3+} ions from tetrahedral A sites to Fe^{2+} ions at octahedral B sites [19].

Several research works have been focused on different preparation routes to synthesize $NiFe_2O_4$ nanoparticles, such as co-precipitation [23], sol-gel [24], spray pyrolysis [25], mechanical activation [26], hydrothermal method [27], high energy ball milling [28], etc.. Concurrently, to improve the physical properties of nanoferrites using γ rays, various methods have been employed to synthesize ferrite nanoparticles. Recently, Raut et al. [19] synthesized $ZnFe_2O_4$ using sol-gel auto-combustion technique and reported that saturation magnetization and magneton number increased by γ radiation dose of 50 and 100 kGy. Raut et al. [29] also prepared $CoFe_2O_4$ by sol-gel auto combustion with total radiation doses of 50 and 100 kGy and showed that lattice parameters decline with Coercivity (H_c), Remanence magnetization (M_r) and anisotropy field (H_k) shrinkages as a function of γ radiation doses. Based on the above survey, till now, there is no study on the impact of γ radiations on $NiFe_2O_4$ nanoparticles synthesized by sol-gel auto combustion method. Therefore, the aim of the research work is to synthesize and investigate some of the physical parameters of $NiFe_2O_4$ before and after γ -irradiation.

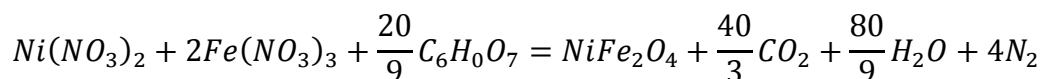
2 Experimental sections

2.1 Materials

In this experiment, Nickel Nitrate Hexahydrate ($Ni(NO_3)_2 \cdot 6H_2O$), Ferric Nitrate Nanohydrate ($Fe(NO_3)_3 \cdot 9H_2O$), Citric Acid ($C_6H_8O_7 \cdot H_2O$), Ammonium Hydroxide (NH_4OH) were used for the sample preparation. The samples were made by mixing the compositions ($Ni(NO_3)_2 \cdot 6H_2O$, $Fe(NO_3)_3 \cdot 9H_2O$, $C_6H_8O_7 \cdot H_2O$ and NH_4OH) together. The required materials were employed as received.

2.2 Synthesis route

Sol-Gel Auto-Combustion route has been employed to prepare the $NiFe_2O_4$ nanoparticles as a function of γ -irradiation for 0, 25 and 100 kGy doses involving the metal nitrates of the ingredient components as raw materials in citric acid matrix. The synthesis route has been explained as follows: the metal nitrates and citric acid were dissolved in an appropriate amount to keep the molar ratio of metal ions and used citric acid to 1:1. A little quantity of ammonia was gradually dissolved into the starting solution to balance $pH = 7$ and stabilize the nitrate-citrate sol. The obtained precursor aqueous solution was stirred vigorously with a magnetic stirrer at 60 °C. After that the sol was placed into a tray and heated gradually to 120 °C to change into an extremely viscous brown gel. The gel was slowly heated to 250 °C in order to attain dried gel and after few minutes, the gel started to completely burnt to form a crisp powder. The probable chemical reaction during the synthesis of $NiFe_2O_4$ products is given as:



2.3 Co-60 Gamma irradiation

The synthesized NiFe₂O₄ products have been subjected to γ -irradiation originated from a ⁶⁰Co source with various doses (25 kGy and 100 kGy) at Institute of Food and Radiation Biology (IFRB), Atomic Energy Research Establishment, Bangladesh Atomic Energy Commission, Dhaka, Bangladesh. The activity of ⁶⁰Co source at the time of exposure is 12.17kGy/h and liquid phase dosimetry arrangement (Cericroous) has been employed to enumerate the γ -dose rate.

2.4 Characterization techniques

The morphological investigation of the products has been acquired by Field Emission Scanning Electron Microscopy (FESEM) (JEOL JSM-7600F, USA). X-ray Diffraction (XRD) (model X'PertPRO XRD Philips PW3040, Netherlands) has been applied on the resulted NiFe₂O₄ and γ -irradiated NiFe₂O₄ to identify the phases and crystallinity. XRD structure is equipped with a Cu-K α radiation ($\lambda = 1.5404 \text{ \AA}$) maintained in the range of 2θ from 15° to 90°. XRD spectra have been investigated through the Rietveld technique as implemented in Fullprof software. To examine the functional groups associated with ferrite samples, Fourier Transform Infrared Spectroscopy (FTIR) equipment has been employed during this experiment. Physical Properties Measurement System (PPMS), Quantum Design Dyna Cool at ambient conditions has been used to measure the magnetic hysteresis loop on the obtained products as well as different magnetic parameters such as saturation magnetization (M_s), remnant magnetization (M_r) and coercive field (H_c). DRS informations has been recorded by a UV–Vis device (Model: PerkinElmer UV–Vis–NIR Spectrometer Lambda 1050) at a wavelength of 200–800 nm.

3 Results and discussion

3.1 Surface morphology properties

Fig. 1 reveals the FESEM images of pristine and γ -irradiated NiFe₂O₄ with comparatively low (25kGy) and high (100 kGy) doses of γ radiations. It is clearly seen in the FESEM images that the surface morphology of NiFe₂O₄ is being altered with total dose of γ radiation. The same outcomes have been detected in the previous literature [30][31][32]. According to the FESEM images [Fig. 1(a,d)], the highest average particle size is pronounced 168 nm for pristine sample. It is seen that result of employing a low γ dose, the surface disrupts and making smaller particles due to the lattice vibration, atomic displacement and local heating effects [33]. The disintegration of particles can also be attributed to induced compressive stress which causes intrinsic defect recombination or reordering of initially disordered phase and aids the particles to regain their shapes [34][35]. In addition, at a low dose, γ photon has a higher possibility of interaction with the materials and then photoelectric absorption dominates, resulting in the decrement of average particle size of NiFe₂O₄ from 168 to 135 nm [36]. Conversely, in case of high dose (100 kGy), the average particle size is slightly increased from 135 to 140 nm as shown in Fig. 1(c,f). The swelling of average particle size may be occurred due to the decrease of photoelectric absorption [37]. It is well known that particles amalgamate at higher γ dose owing to no electron transfer,

thereby, to make sure increment of average particle size [38]. A hypothetical growth mechanism of NiFe_2O_4 particles in pristine and γ -irradiated samples with different γ doses is depicted in Fig. 2.

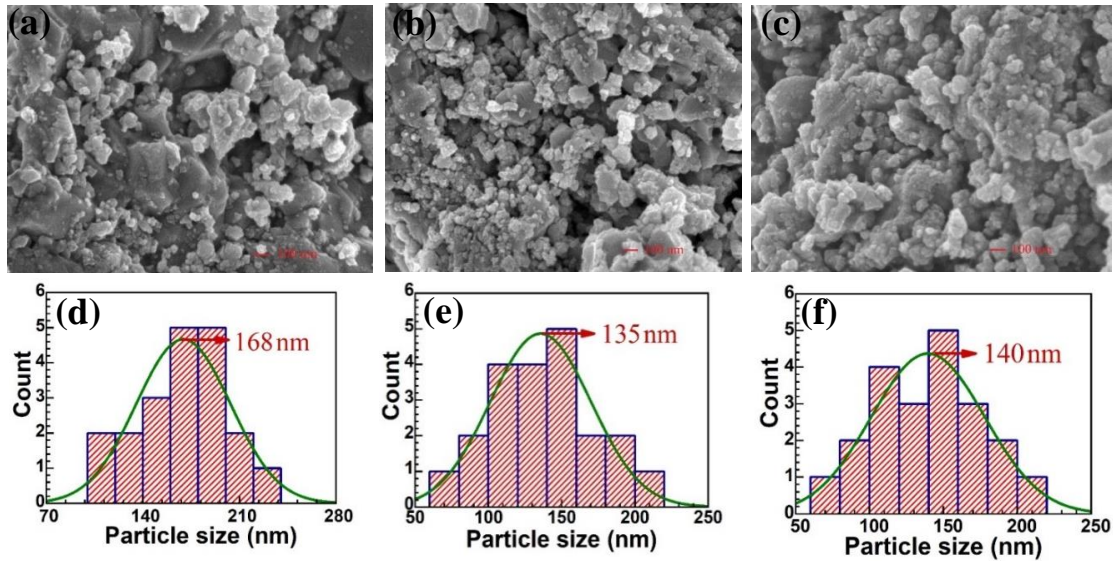


Fig. 1 The FESEM images and particle size distribution of NiFe_2O_4 samples: (a, d) for 0 kGy, (b, e) for 25kGy, and (c, f) for 100 kGy doses.

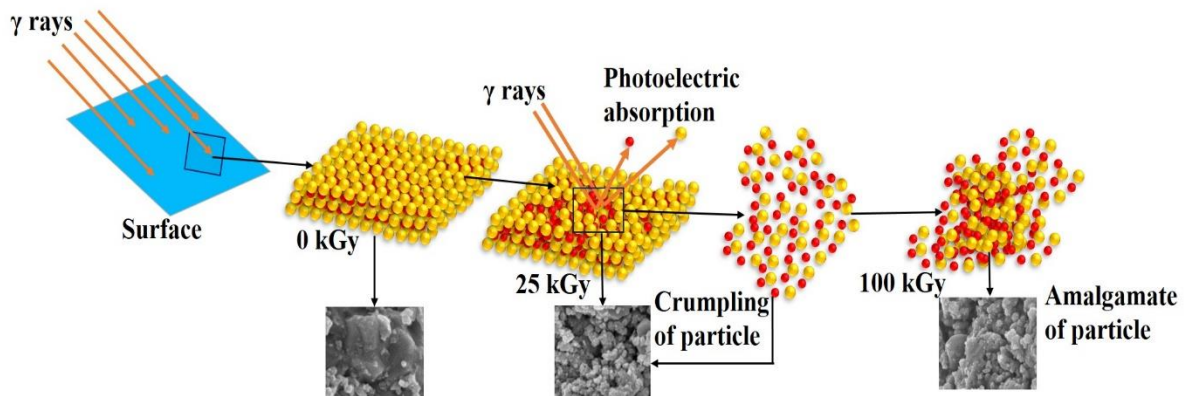


Fig. 2 A plausible growth mechanism of pristine and γ -irradiated NiFe_2O_4 samples.

3.2 Structural properties

Fig. 3 depicts the Rietveld refinement (R.R) of the structure by XRD data is processed using Fullprof suite software. By a meticulous R.R analysis, a dual common inverse spinel cubic structure ($Fd\bar{3}m$) and hematite phase ($R\bar{3}c$) is firmly confirmed for the pristine and irradiated samples. It can be evidently indexed to the face centered cubic (fcc) structure of NiFe_2O_4 (JCPDS Card No.10-0325) [39] as shown in Fig. 3. On the other hand, a nickel phase ($Fm\bar{3}m$) has appeared for only the irradiated samples. From Fig. 3, it can be seen that the most prominent intense peak is manifested at $2\theta = 35.74^\circ$ corresponding to the (311) plane of NiFe_2O_4 for

pristine sample. After that, the place of (311) plane orientation has been changed from $2\theta = 35.75^\circ$ to 35.79° by applying gamma radiation. This may be attributed to the formation of Fe^{3+} ions in the place of Fe^{2+} ions. It is also noticeable that the intensity of (3 1 1) peak increases while (400) peak intensity decline for applying 25 kGy gamma radiation. Conversely, owing to 100 kGy gamma radiation, the intensity of (400) peak rises sharply when (311) peak falls drastically. Such results, the shift of the peak intensity is in good agreement with that reported by several authors and they ascribed that to the lattice distortion arisen after irradiation [40][41].

To know the lattice parameters, we have done the R.R analysis using the FullProf software. The quality of the R.R is determined by means of a set of conventional statistical parameters. Typically, the quality of the R.R can be determined using several statistical parameters such as goodness of fit (χ^2), weight Profile R-factor (R_{wp}) and expected R-Factor (R_{exp}), whereas R_{wp} comparisons the adjusted data with the experimental data, R_{exp} estimates the quality of the experimental data and $\chi^2 = \left(R_{wp} / R_{exp} \right)^2$ [42]. During the R.R process, χ^2 initiates with a maximum value when the goodness of fit model is poor and decreases as the fit data matches the experimental data.

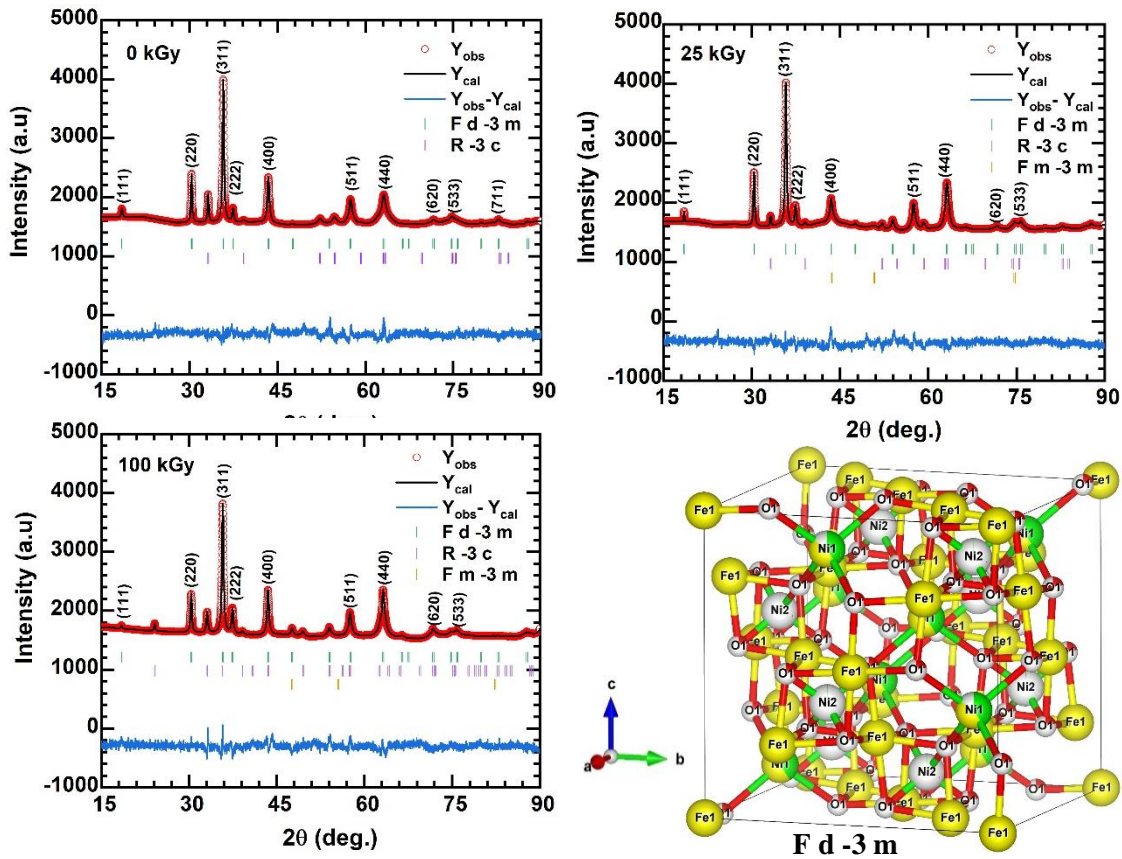


Fig. 3 The Rietveld refinement of XRD pattern with different γ irradiations and a face centered cubic (fcc) structure of NiFe_2O_4

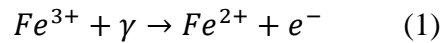
Table 1 Several structural parameters of pristine and γ -irradiated samples

| Parameters | | 0 kGy | 25 kGy | 100 kGy | | | |
|------------------------------------|--|----------------------------------|----------------------------------|-------------------------------|-----------------------------|----------------|----------|
| Lattice constants (\AA) | NiFe ₂ O ₄ ($a = b = c$) | 8.3304 | 8.3268 | 8.3189 | | | |
| | Fe ₂ O ₃ ($a = b, c$) | 5.4033, 5.2724 | 5.4022, 5.3045 | 5.0309, 13.7998 | | | |
| | Ni ($a = b = c$) | --- | 3.5980 | 3.3129 | | | |
| Volume (\AA^3) | NiFe ₂ O ₄ | 578.1011 | 577.3437 | 575.7062 | | | |
| | Fe ₂ O ₃ | 133.3125 | 134.0625 | 302.4775 | | | |
| | Ni | --- | 46.5782 | 36.3614 | | | |
| Crystallite size (nm) | D _{D-S} | 34.04 | 34.71 | 34.12 | | | |
| | D _{ave.} | 24.55 | 51.16 | 42.61 | | | |
| | D _{W-H} | 71.23 | 83.23 | 77.78 | | | |
| | D _{R-R} | 70.12 | 77.78 | 75.01 | | | |
| Rietveld Refinement | R _{wp} (%) | 8.10 | 8.04 | 8.07 | | | |
| | R _{exp} (%) | 6.95 | 7.04 | 6.98 | | | |
| | G.O.F (χ) | 1.69 | 1.88 | 1.56 | | | |
| | Oxygen position, (u) | 0.22920 | 0.25356 | 0.39745 | | | |
| Bond length (\AA) | NiFe ₂ O ₄ | Fe-O | 1.92552 | 2.11176 | 3.29151 | | |
| | | Fe-Fe | 2.94526 | 2.94397 | 2.94120 | | |
| | | Ni ₁ -O | 2.10304 | 1.75146 | --- | | |
| | | Ni ₂ -O | 1.50415 | 1.85415 | --- | | |
| | | Ni ₁ -Ni ₂ | 4.16522 | 4.16340 | 4.15953 | | |
| | | Ni ₁ -Fe | 3.45362 | 3.45211 | 3.44882 | | |
| | Fe ₂ O ₃ | Fe-O | 1.4709, 1.5088, 1.5270, 2.2582 | 1.8016, 2.0098 | 1.8154, 2.1871 | | |
| | | | 1.5270 | 2.1372 | 3.4068, 2.9507 | | |
| | | Ni ₂ | Ni-Ni | ---- | 2.5442, 3.5981 | 2.3426, 3.3129 | |
| | | | O-Fe-O | 79.28, 100.72, 100.75, 100.73 | 88.40, 91.60, | 9.20, | |
| | | Bond angle (deg.) | NiFe ₂ O ₄ | O-Ni ₁ -O | 109.45, 109.47, 109.48 | 109.4712 | 109.4712 |
| | | | | O-Ni ₂ -O | 109.51, 109.48, 109.45 | 109.4712 | --- |
| Fe-O-Ni ₁ | 117.96 | | | 126.40 | 116.67 | | |
| Fe ₂ O ₃ | Fe-O-Ni ₂ | | 62.03 | 53.60 | O-Fe-Ni ₂ =98.60 | | |
| | Fe-O-Fe | | 61.6417 | 67.9588 | 71.4986 | | |
| | O-Fe-O | | 85.9783 | 78.7610 | 85.4653 | | |

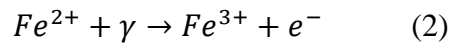
The R.R process continues until convergence is reached with values less than 2.0 or close to 1.0, which designates a correlation between the experimental data and adjustment model used. The values of R_{wp} , R_{exp} , and χ^2 are presented in Table 1. In addition, the estimated Rietveld refined lattice parameter and volume values are also tabulated in Table 1. It can be seen (Table 1) that both the lattice parameter and volume are decreasing simultaneously with increasing the gamma radiations which signifies that atomic position is displaced significantly. The shrinking of lattice parameter and volume due to the lattice vacancies produced after γ radiation dose reasons distortion and deviation from the spinel cubic structure. Besides, γ radiation typically formed the compressive strain and then generated some disorder into the $NiFe_2O_4$ lattice structure [43].

However, the crystallite size of the samples is calculated from the line width of the (3 1 1) peak using Debye-Scherrer's (D-S) equation [44]: $D_{D-S} = \frac{k\lambda}{\beta \cos\theta}$, where ' D_{D-S} ' is the crystallite size, ' λ ' is the wavelength of $CuK\alpha$ radiation (1.5404Å), ' β ' is the full width half maxima (FWHM), and ' θ ' is the diffraction angle of the strongest characteristic peak. After that, we have also estimated the average crystallite size ($D_{ave.}$) using the Lorentz function by Origin pro-2018. From Table 1, it is clearly evident that in both cases the D_{D-S} and $D_{ave.}$ increases drastically at 0 and 25 kGy samples, and decreases at the 100 kGy sample. To get the more accurate crystallographic parameters such as crystallite size, strain, atomic structure, bond length and bond angle, the Williamson–Hall (W-H) method and Rietveld refinement (R.R) is performed precisely. Initially, the W-H method gives the values of crystallite size and strain concurrently.

The equation of W-H method is [45]: $\beta \cos\theta = 4\varepsilon_{WH} \sin\theta + \frac{K\lambda}{D_{WH}}$, where is an intercept in W-H plot that corresponds to the crystallite size (DW–H) and slope ε_{W-H} corresponds to the strain as shown in Fig. 4. It can be seen that D_{W-H} lies between 71.23 to 83.23 nm which emulates the D_{D-S} and D_{ave} trend. Additionally, the Rietveld refined (R-R) crystallite size is found from 70.12 to 77.78 nm. It is observed that the crystallite size increases after 25 kGy γ radiation doses, which is ascribed to the following: γ radiation interacts with the particles or grains and ionizes Fe^{3+} ions to Fe^{2+} ions [46] as follows:



But the crystallite size decreases at 100 kGy γ radiation dose due to the modification of the ratio of Fe^{2+}/Fe^{3+} ions in octahedral-B site that can be expressed by the following equation [47]:



Through the R-R analysis, we have determined the bond length and bond angle to know the gamma radiation effect into the $NiFe_2O_4$ structure. Firstly, in the case of $NiFe_2O_4$, the Fe-O and Ni_2 -O bond length is grown up abruptly while Fe-Fe, Ni_1 -O, Ni_1 - Ni_2 , Ni_1 -Fe and Ni_2 -Fe bond distance declining after using gamma radiations as shown in Table 1 and Fig. 5.

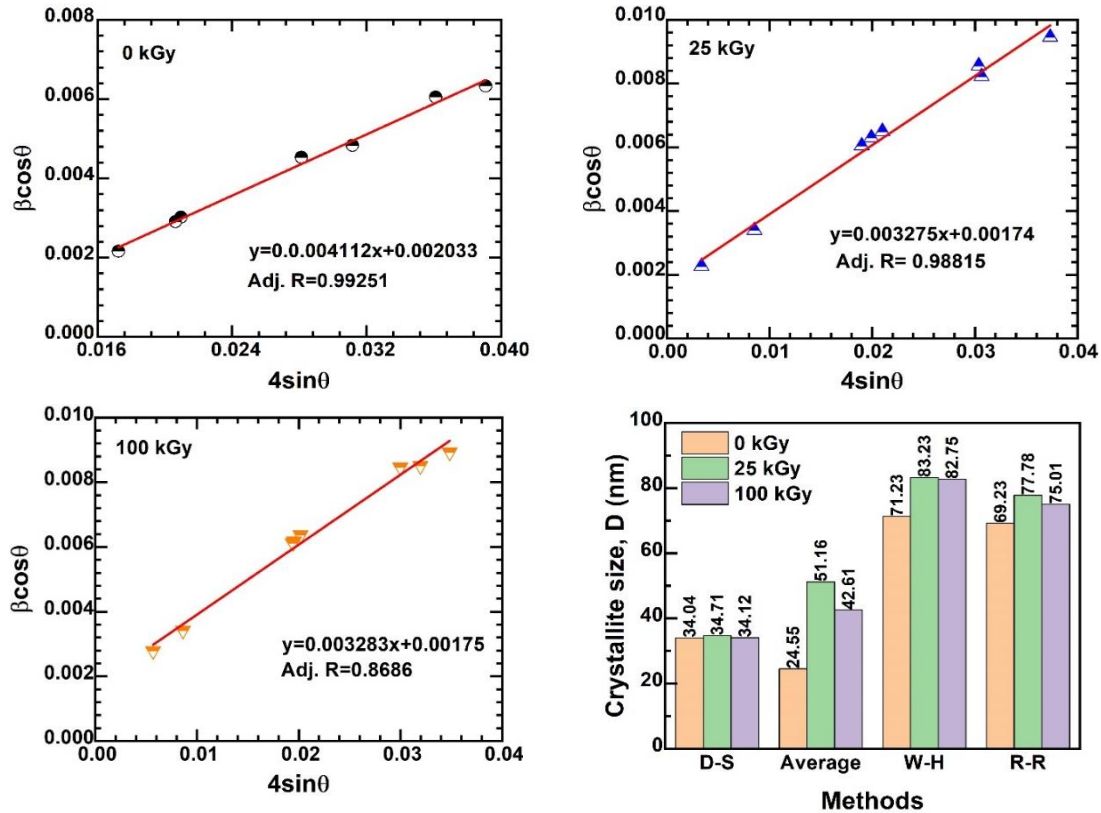


Fig. 4 Williamson–Hall plot for NiFe₂O₄ with different γ irradiations. A comparison crystallite size studies among various methods.

Interestingly, there is no bond length appeared between Ni₁-O and Ni₂-O at 100 kGy sample that may be attributed to the development of Fe-O bond distance. Further, multiple bond distance of Fe-O, Fe-Fe and Ni-Ni is detected for Fe₂O₃ and Ni structures as shown Table 1. Likewise, in the event of a bond angle, we have found multiple bond angles in the NiFe₂O₄ and Fe₂O₄ structures. The O-Ni₁-O and O-Ni₂-O bond angle almost analogous, on the contrary, Fe-O-Ni₁ and Fe-O-Ni₂ bond angle completely different in the NiFe₂O₄ structure. What's more, an interest point has build that Ni₂ atom does not make bond length and bond angle as well at 100 kGy sample. It can be speculated that owing to the higher gamma radiation Ni₂-O bond split up and then make a new bond only with the Fe atom as shown in Fig. 5.

However, the Hopping length (distance between magnetic ions in tetrahedral site-L_A and octahedral sites-L_B) is another important structural parameter which estimated by these equations [48]: $L_A = \frac{1}{4}a\sqrt{3}$ and $L_B = \frac{1}{4}a\sqrt{2}$, where 'a' is the lattice parameter of NiFe₂O₄ structure. The calculated values of the L_A and L_B are presented in the Table 2. It is seen (Table 2) that the hopping lengths in L_A and L_B sites decrease concurrently with changing gamma radiations. But other groups showed that in the case of ZnFe₂O₄ and CoFe₂O₄, hopping lengths increased after using gamma radiations as they have found greater values of lattice parameters [19][29].

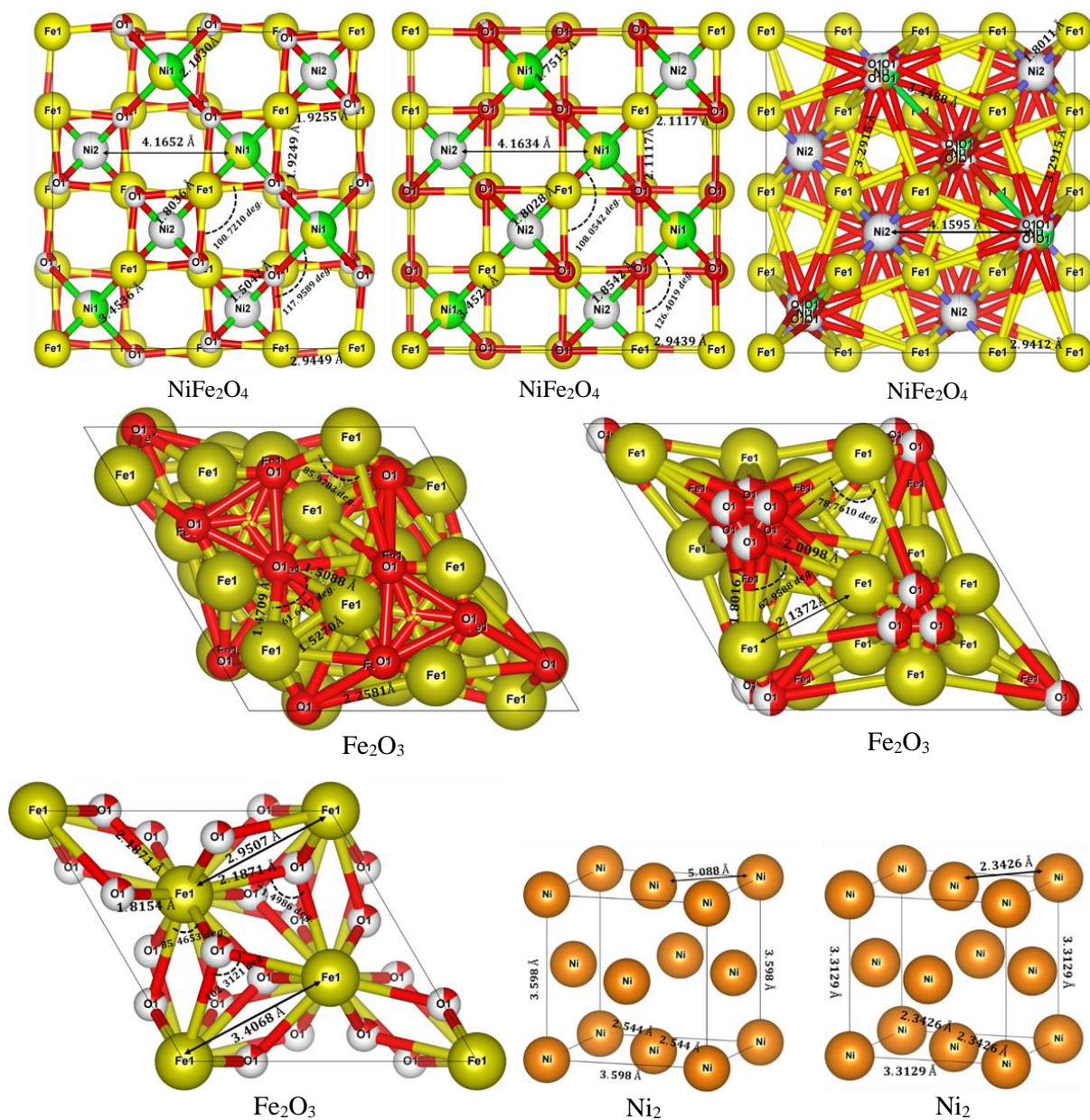


Fig. 5 Several Rietveld refined structures with denoting bond lengths and bond angles.

In the present study, the lattice parameter, volume, and bond length are shrunk with altering gamma radiations which are firmly confirmed that these structural parameters control the Hopping lengths. Further, the inter-ionic distances (average bond lengths) at tetrahedral- R_A and octahedral sites- R_B is calculated using the following relations [49]:

$$R_A = a\sqrt{3}\left(u - \frac{1}{4}\right) \quad (3)$$

$$R_B = a\sqrt{3u^2 - 2u + \frac{1}{16}} \quad (4)$$

Where ‘u’ represents the Rietveld refined oxygen positional parameter which values are 0.22920, 0.25356 and 0.39745 for 0, 25 and 100 kGy gamma radiation samples, respectively. Our refined ‘u’ values are analogous with previous reported data [50]. But other groups have been taken theoretical value of oxygen position parameter ($u=0.381\text{\AA}$). Patange et al. has chosen ‘u’ value for Al^{3+} substituted NiFe_2O_4 nanoparticles despite the Rietveld refinement analysis [51]. It is observed that ‘u’ is increased with rising gamma radiations, and R_A is increased while declining R_B as shown in Table 2.

Table 2 The estimated Hopping lengths and average bond length of NiFe_2O_4 for various γ irradiations

| Parameters | | 0 kGy | 25 kGy | 100 kGy |
|--------------------------------------|----------------------------|--------|--------|---------|
| Hopping length (\AA) | L_a | 3.6072 | 3.6056 | 3.6022 |
| | L_b | 2.9445 | 2.9440 | 2.9412 |
| Average bond length (\AA) | Tetrahedral site (R_A) | 1.5035 | 1.8542 | 3.9257 |
| | Octahedral sites (R_B) | 2.2691 | 2.0525 | 1.9331 |

The change of R_A and R_B can be explained on the basis of the drastic movement of oxygen position parameters. Since oxygen position is developed considerably with rising gamma radiations, so the NiFe_2O_4 structure becomes slowly close to the fcc structure and oxygen ions are moving towards octahedral coordinated at the end. However, several studies are investigated on spinel ferrite by gamma doses. Here, we have reported on the effect of gamma dose over several spinel ferrites in Table 3.

Table 3 A comparison study for various spinel ferrites under γ irradiations

| Sample | Rietveld refinement | No. of phases | Lattice constant | Determined bond length and bond angle | Determined R_A and R_B | Hopping length | Ref |
|---------------------------|---------------------|---------------|------------------|---------------------------------------|----------------------------|----------------|---------|
| ZnFe_2O_4 | No | Single | Increase | No | No | Increase | [19] |
| CoFe_2O_4 | No | Single | Increase | No | No | Increase | [29] |
| NiFe_2O_4 | Yes | Three | Decrease | Yes | Yes | Decrease | present |

3.3 Optical properties

The optical band gap (E_g) of the pristine and γ -irradiated NiFe_2O_4 samples has been calculated from the Kubelka–Munk (K–M) function through the following equation [52]:

$$F(R) \propto \alpha = \frac{(h\nu - E_g)^2}{h\nu} \quad (5)$$

Where, ‘R’ is the reflectance, ‘ α ’ is the absorption coefficient, ‘ $h\nu$ ’ is the incident light energy and ‘ E_g ’ is the optical band gap. Fig. 6 shows the E_g plots of the NiFe_2O_4 treated with different γ irradiation doses. The E_g is calculated by plotting a graph between $(F(R) \times h\nu)^2$ versus $h\nu$. In the pristine NiFe_2O_4 , the E_g is 1.85 eV. Subsequently, for 25 and 100 kGy irradiation doses, the E_g is found to be 1.80 and 1.89 eV, respectively. Thus, we observe that the E_g shrinkages when

low doses of γ irradiation are used, while with high dose γ irradiation the E_g is increased. The change in E_g can be expounded by the following ways: (i) quantum-size effect may be accountable for altering the E_g . Because it is resulting from the strong interaction between the surface of NiFe_2O_4 and γ photons [53].

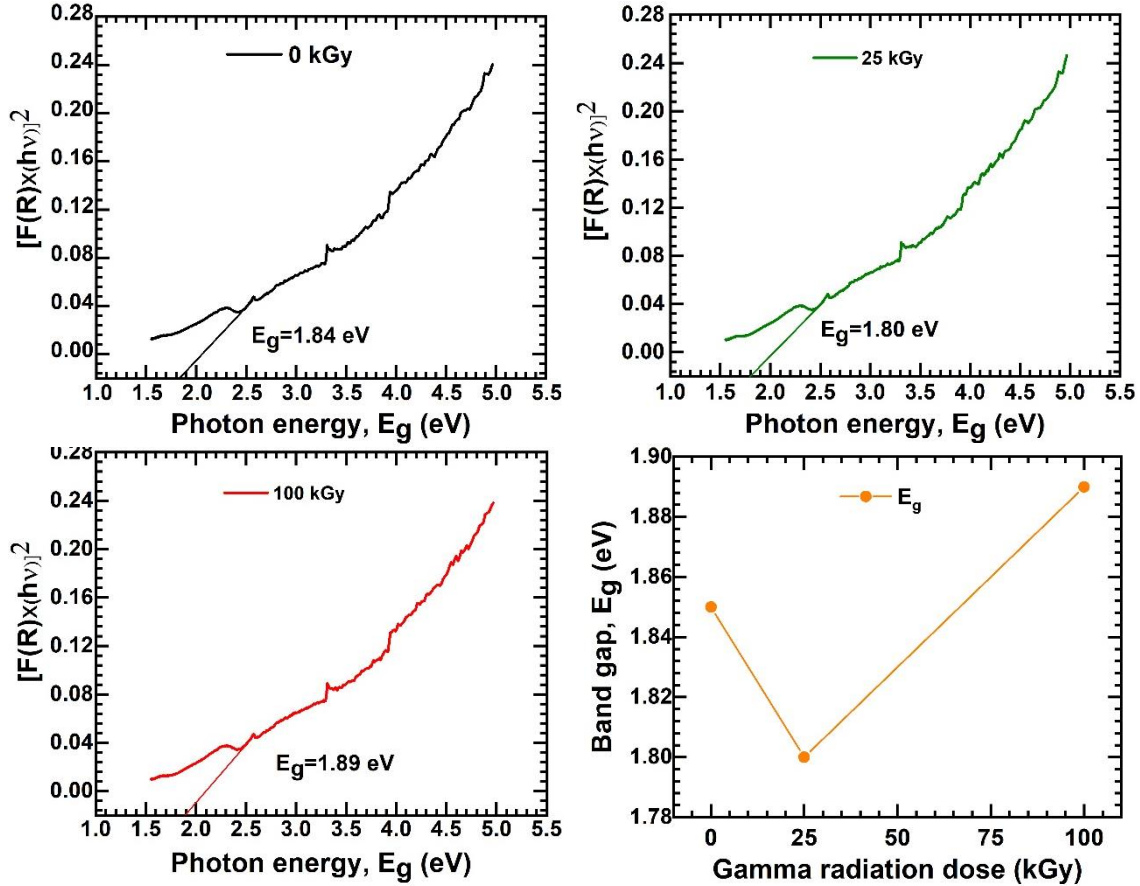


Fig. 6 The E_g of NiFe_2O_4 with various γ irradiation doses and with that a comparison of E_g study

(ii) decrease of E_g may be ascribed to the creation of localized states into the NiFe_2O_4 structure due to structural defects [54]. (iii) enhancement of E_g due to the optical scattering at the particle or grain boundaries and intrinsic absorption [21]. Besides, it is anticipated that the \dot{V}_O is created within NiFe_2O_4 structure during higher dose of γ irradiation that will play a significant role to increase the E_g [55]. However, it is manifested that the γ irradiation significantly affects the crystallite size and hence alter the optical band gap of NiFe_2O_4 .

3.4 FTIR analysis

Fig. 7 displays the FTIR diagram of pristine NiFe_2O_4 and NiFe_2O_4 irradiated with γ -doses for analysis of chemical bonds within the resulted products. The prominent bands with sharp peaks have been observed at 365 cm^{-1} and 547 cm^{-1} which are assigned to stretching vibrations of Ni-O bond in octahedral complexes and tetrahedral Fe-O vibrations, respectively [56][57]. This analysis of FTIR presents the consistency with published results in numerous bodies of literature

[58][59][60] and ensures the construction of the spinel NiFe_2O_4 nanoparticles identifying characteristic peaks in FTIR diagram. The FTIR studies clearly support the formation of Ni ferrite as observed in XRD analysis. The presence of band positions in the ranges of $1000\text{--}1300\text{ cm}^{-1}$ and $2000\text{--}3000\text{ cm}^{-1}$ demonstrates the survival of O–H, C–O, and C=H stretching mode of organic compounds [61]. Two peaks appear at 1381 cm^{-1} and 3754 cm^{-1} in case of the pristine and γ -irradiated products, which belongs to stretching vibration of C–H and the contribution of N–H bonds, respectively [61].

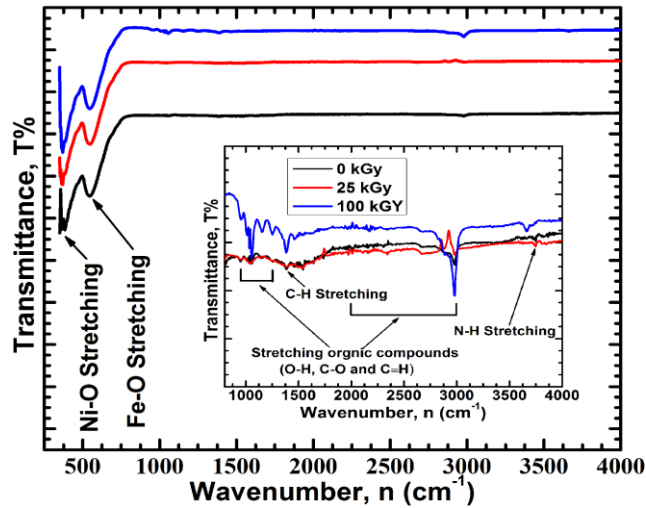


Fig. 7 FTIR spectra of pristine and γ -irradiated NiFe_2O_4

3.5 Magnetic properties

Fig. 8 shows the room temperature magnetization (M) for the applied field (H) of as-prepared NiFe_2O_4 nanoparticles before (0 kGy) and after irradiation (25 kGy and 100 kGy). The applied field was ranged from -20 kOe to $+20\text{ kOe}$, and it is apparent that the magnetization is not saturated at 20 kOe . Low coercivity and low hysteresis indicates the ferrimagnetic behavior of the samples. The magnetic parameters such as saturation magnetization (M_s), Remanence (M_r) and coercivity (H_c) are summarized in Table 4. The saturation magnetization (M_s) was found for the pristine sample was $\sim 28\text{ emu/g}$, which is less than the bulk NiFe_2O_4 . It can be attributed to the fact that NiFe_2O_4 becomes mixed spinel from the inverse spinel structure at the nanoscale [62].

The tetrahedral A-site consists of ferromagnetically ordered Fe^{3+} ions, and the octahedral B-site consists of Fe^{3+} and Ni^{2+} ions. The magnetic contribution in the inverse spinel arises from the Ni^{2+} in the octahedral B-site. Due to antiferromagnetic ordering, the Fe^{3+} moments from both the A-site and B-site cancel each other. Considering the magnetic moments of Fe^{3+} and Ni^{2+} ions are $5\mu_B$ and $2\mu_B$, the net magnetic moment is $2\mu_B$ by Neel's two sublattice model [63]. Therefore, the proposed change in the cation distribution at the nanoscale can be interpreted as $(\text{Ni}_x\text{Fe}_{1-x})_A[\text{Ni}_{1-x}\text{Fe}_{1+x}]_B$. However, the presence of Ni^{2+} might not be that dominant in the tetrahedral A-site for the pristine samples. Also, the synthesis methods significantly impact the magnetic properties on spinel ferrites [64].

There is an increment in the M_s from 28 emu/g to 41 emu/g after the γ –irradiation of 25 kGy. After the γ –irradiation, the degree of mixed-phase may have increased, and more Ni^{2+} has transferred to the A-site. Also, the irradiation releases the pinned domains on the surface, and the significant increment of magnetization was observed [65][66]. Furthermore, the onset of crystallite size growth was observed after the irradiation. Crystallite size growth may accompany the migration of Fe^{3+} ions to the B-site [2][67]. The decreasing trend in the lattice parameter also established the emergence of strong ionic interactions among the lattice sites. Therefore, the enhanced saturation magnetization was observed.

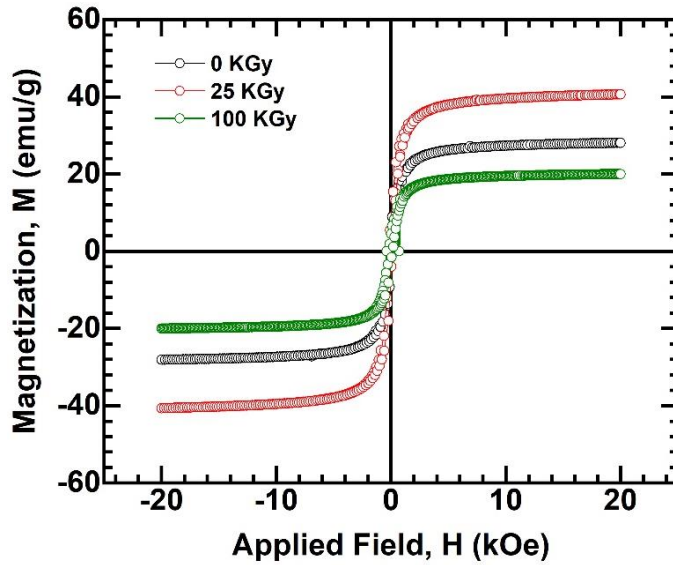


Fig. 8 M-H curves of the pristine and γ –irradiated samples of $NiFe_2O_4$.

Consequently, it will be interesting to investigate the magnetic properties on exposing the samples at higher γ –radiation. However, a strong γ –irradiation of 100 kGy decreased the M_s drastically to 20 emu/g. The strong γ –irradiation causes the adverse effect on magnetic ordering by the ion-induced disorder. Also, high energy ions may penetrate the sample. The host atoms and molecules interact with the irradiated gamma photons via inelastic collision.

Table 4 Magnetic parameters of pristine and γ -irradiated samples of $NiFe_2O_4$

| Radiation (kGy) | M_s (Ex) (emu/g) | Remanence, M_r (emu/g) | Coercivity, H_c (Oe) |
|-----------------|--------------------|--------------------------|------------------------|
| 0 | 28.08 | 4.87 | 0.0022 |
| 25 | 40.63 | 8.44 | 0.0303 |
| 100 | 20.00 | 4.87 | 0.0216 |

The interaction causes energy loss and introduces defects or partial amorphization depending on the amount of energy lost [68]. Hence, a decrease in crystallite size was observed. The reduction of crystallite size introduces spin canting, magnetic dead layers and weakening of super-

exchange interaction. Consequently, a substantial reduction in saturation magnetization has emerged.

4 Conclusions

Nanoparticles NiFe₂O₄ ferrites in spinel cubic structure have been synthesized via sol-gel auto-combustion route. We have investigated the structural, morphological, magnetic and optical properties of the resultant ferrite nanoparticles with the variation of γ -doses. FESEM micrographs clearly indicate the variation in morphology and aggregation nature within the bare and γ -irradiated Ni ferrite products. According to the XRD investigation of the conducted research, it is concluded that an irregular variation in crystallite size leads from the results of Scherrer method. In addition, analysis of the W-H plot and R-R exhibit the identical trend of variation upon incorporation of γ -irradiation into the NiFe₂O₄ crystal network. The crystallite size of pristine Ni ferrite sample is observed as 24.55 nm-71.23 nm. The result after γ -irradiation with 25 kGy shows the increment nature of crystallite size and then decrease after exposure to high γ -dose (100 kGy). From the Rietveld analysis numerous structural parameters such as bond length, bond angle, hopping length etc. are estimated in this current study. The optical bandgap energy is estimated at 1.85 eV in the pristine product and consequently, in the case of low (25kGy) and high (100 kGy) γ -doses it corresponds to be 1.80 and 1.89 eV, respectively. Two absorption bands located at 365 cm⁻¹ and 547 cm⁻¹ have been detected from the FTIR measurement which indicates the stretching vibrations at the octahedral site of Ni-O and tetrahedral Fe-O vibrations, respectively. This obtained observation confirms the formation of spinel cubic phase in both pristine and γ -irradiated Ni ferrites nanoparticles supported by XRD results. PPMS measurement reveals that the M_S value for pristine product is noticed as 28.08 emu/g. A considerable increase in saturation magnetization from 28.08 emu/g to 40.63 emu/g in low γ -irradiated compound (25 kGy) which may be due to the surface canting effect affected by the agglomeration nature of ferrite particle and then decreasing nature after exposure to high γ -dose.

References

- [1] R.M. Anderson, C.R. Vestal, A.C.S. Samia, Z.J. Zhang, Faraday rotation in Co_{0.85}Zn_{0.15}Fe₂O₄ spinel ferrite nanoparticulate films under low applied fields, *Appl. Phys. Lett.* 84 (2014) 3115. doi:10.1063/1.1712031.
- [2] D.S. Nikam, S. V. Jadhav, V.M. Khot, R.A. Bohara, C.K. Hong, S.S. Mali, S.H. Pawar, Cation distribution, structural, morphological and magnetic properties of Co_{1-x}Zn_xFe₂O₄ (x = 0-1) nanoparticles, *RSC Adv.* 5 (2015) 2338–2345. doi:10.1039/c4ra08342c.

- [3] E. Rezlescu, L. Sachelarie, P.D. Popa, N. Rezlescu, Effect of Substitution of Divalent Ions on the Electrical and Magnetic Properties of Ni–Zn–Me Ferrites, *IEEE Trans. Magn.* 36 (2000) 3962–3967.
- [4] C. Xiangfeng, L. Xingqin, M. Guangyao, Preparation and gas sensitivity properties of ZnFe₂O₄ semiconductors, *Sensors Actuators B.* 55 (1999) 19–22.
- [5] B.U. Lüders, A. Barthélémy, M. Bibes, K. Bouzehouane, S. Fusil, E. Jacquet, J. Contour, J. Bobo, J. Fontcuberta, A. Fert, NiFe₂O₄ : A Versatile Spinel Material Brings New Opportunities for Spintronics, *Advanced Mater.* 18 (2006) 1733–1736. doi:10.1002/adma.200500972.
- [6] X. Gu, W. Zhu, C. Jia, R. Zhao, W. Schmidt, Y. Wang, Synthesis and microwave absorbing properties of highly ordered mesoporous crystalline NiFe₂O₄, *Chem. Commun.* 47 (2011) 5337–5339. doi:10.1039/c0cc05800a.
- [7] R. Benrabaa, A. Löfberg, A. Rubbens, E. Bordes-richard, R.N. Vannier, A. Barama, Structure, reactivity and catalytic properties of nanoparticles of nickel ferrite in the dry reforming of methane, *Catal. Today.* 203 (2013) 188–195. doi:10.1016/j.cattod.2012.06.002.
- [8] Y. Fu, Y. Wan, H. Xia, X. Wang, Nickel ferrite-graphene heteroarchitectures : Toward high-performance anode materials for lithium-ion batteries, *J. Power Sources.* 213 (2012) 338–342. doi:10.1016/j.jpowsour.2012.04.039.
- [9] A. Sutka, The Role of Stoichiometry on Gas Response of Nanostructured Sol–Gel Auto Combustion Derived Nickel Ferrite, *Sens. Lett.* 11 (2013) 2010–2013. doi:10.1016/j.mssp.2020.105220.
- [10] H. Yin, H.P. Too, G.M. Chow, The effects of particle size and surface coating on the cytotoxicity of nickel ferrite, *Biomaterials.* 26 (2005) 5818–5826. doi:10.1016/j.biomaterials.2005.02.036.
- [11] A. Shan, X. Wu, J. Lu, C. Chen, R. Wang, Phase formations and magnetic properties of single

- crystal nickel ferrite (NiFe₂O₄) with different morphology, *CrystEngComm*. 17 (2015) 1603–1608. doi:10.1039/x0xx00000x.
- [12] H. Perron, T. Mellier, C. Domain, J. Roques, E. Simoni, R. Drot, C. H, Structural investigation and electronic properties of the nickel ferrite NiFe₂O₄: a periodic density functional theory approach, *J. Phys. Condens. Matter*. 19 (2007) 346219. doi:10.1088/0953-8984/19/34/346219.
- [13] C.N. Chinnasamy, A. Narayanasamy, N. Ponpandian, K. Chattopadhyay, K. Shinoda, B. Jeyadevan, K. Tohji, K. Nakatsuka, T. Furubayashi, I. Nakatani, Mixed spinel structure in nanocrystalline NiFe₂O₄, *Phys. Rev. B - Condens. Matter Mater. Phys.* 63 (2001) 184108. doi:10.1103/PhysRevB.63.184108.
- [14] A.B. Nawalea, N.S. Kanhe, K.R. Patil, S. V. Bhoraskar, V.L. Mathe, A.K. Das, Magnetic properties of thermal plasma synthesized nanocrystalline nickel ferrite (NiFe₂O₄), *J. Alloys Compd.* 509 (2011) 4404–4413. doi:10.1016/j.jallcom.2011.01.057.
- [15] S.N. Dolia, P.K. Sharma, M.S. Dhawan, S. Kumar, A.S. Prasad, A. Samariya, S.P. Pareek, R.K. Singhal, K. Asokan, Y.T. Xing, M. Alzamora, E. Saitovitach, Swift heavy ion irradiation induced modifications in magnetic and dielectric properties of Mn – Ca ferrite, *Appl. Surf. Sci.* 258 (2012) 4207–4211. doi:10.1016/j.apsusc.2011.06.011.
- [16] M.A. Ahmed, S.T. Bishay, F.A. Radwan, γ irradiation effect on the polarization and resistance of Li-Co-Yb-ferrite, *J. Phys. Chem. Solids*. 63 (2002) 279–286.
- [17] Y. Ito, K. Yasuda, R. Ishigami, S. Hatori, O. Okada, K. Ohashi, S. Tanaka, Magnetic flux loss in rare-earth magnets irradiated with 200 MeV protons, *Nucl. Instruments Methods Phys. Res. Sect. B*. 183 (2001) 323–328. doi:10.1007/s00339-020-03737-6.
- [18] N. Okasha, Enhancement of magnetization of Mg–Mn nanoferrite by γ - irradiation, *J. Alloy. Compd. J.* 490 (2010) 307–310. doi:10.1016/j.jallcom.2009.10.001.

- [19] A. V Raut, Structural and magnetic characterization of 100-kGy Co 60 γ -ray-irradiated ZnFe₂O₄ NPs by XRD, W – H plot and ESR, *J. Sol-Gel Sci. Technol.* 79 (2016) 1–11. doi:10.1007/s10971-016-4019-y.
- [20] M.F. Desrosiers, Irradiation applications for homeland security, *Radiat. Phys. Chem.* 71 (2004) 479–482. doi:10.1016/j.radphyschem.2004.03.084.
- [21] S.K. Sen, T.C. Paul, S. Dutta, M.A. Matin, M.F. Islam, M.A. Hakim, Effect of gamma (γ -) irradiation on the structural, morphological, optical and electrical properties of spray pyrolysis-deposited h-MoO₃ thin films, *Surfaces and Interfaces.* 17 (2019) 100377. doi:10.1016/j.surfin.2019.100377.
- [22] O.M. Hemedat, M. El-saadawy, Effect of gamma irradiation on the structural properties and diffusion coefficient in Co–Zn ferrite, *J. Magn. Magn. Mater.* 256 (2003) 63–68.
- [23] P. Sivakumar, R. Ramesh, A. Ramanand, S. Ponnusamy, C. Muthamizhchelvan, Synthesis and characterization of NiFe₂O₄ nanosheet via polymer assisted co-precipitation method, *Mater. Lett.* 65 (2011) 483–485. doi:10.1016/j.matlet.2010.10.056.
- [24] P. Lavela, J.L. Tirado, CoFe₂O₄ and NiFe₂O₄ synthesized by sol–gel procedures for their use as anode materials for Li ion batteries, *J. Power Sources.* 172 (2007) 379–387. doi:10.1016/j.jpowsour.2007.07.055.
- [25] D.S. Jung, Y.C. Kang, Effects of precursor types of Fe and Ni components on the properties of NiFe₂O₄ powders prepared by spray pyrolysis, *J. Magn. Magn. Mater.* 321 (2009) 619–623. doi:10.1016/j.jmmm.2008.10.008.
- [26] Z.H. Zhou, J.M. Xue, J. Wang, H.S.O. Chan, T. Yu, Z.X. Shen, NiFe₂O₄ nanoparticles formed in situ in silica matrix by mechanical activation, *J. Appl. Phys.* 91 (2002) 6015–6020. doi:10.1063/1.1462853.

- [27] M. Fu, Q. Jiao, Y. Zhao, Preparation of NiFe₂O₄ nanorod–graphene composites via an ionic liquid assisted one-step hydrothermal approach and their microwave absorbing properties, *J. Mater. Chem. A*. 1 (2013) 5577–5586. doi:10.1039/c3ta10402h.
- [28] T.F. Marinca, I. Chicinaş, O. Isnard, V. Pop, F. Popa, Synthesis, structural and magnetic characterization of nanocrystalline nickel ferrite—NiFe₂O₄ obtained by reactive milling, *J. Alloys Compd.* 509 (2011) 7931–7936. doi:10.1016/j.jallcom.2011.05.040.
- [29] A. V Raut, D. V Kurmude, S.A. Jadhav, D.R. Shengule, K.M. Jadhav, Effect of 100 kGy γ -irradiation on the structural, electrical and magnetic properties of CoFe₂O₄ NPs, *J. Alloys Compd.* 676 (2016) 326–336. doi:10.1016/j.jallcom.2016.03.212.
- [30] S.K. Sen, A. Al Mortuza, M.S. Manir, M.F. Pervez, S.M.A.I. Hossain, S. Alam, M.A.S. Haque, M.A. Matin, M.A. Hakim, A. Huda, Structural and optical properties of sol-gel synthesized h-MoO₃ nanorods treated by gamma radiation, *Nano Express*. 1 (2020) 020026.
- [31] S.K. Sen, M. Noor, M.A. Al Mamun, M.S. Manir, M.A. Matin, M.A. Hakim, S. Nur, S. Dutta, An investigation of ⁶⁰Co gamma radiation-induced effects on the properties of nanostructured α -MoO₃ for the application in optoelectronic and photonic devices, *Opt. Quantum Electron.* 51 (2019). doi:10.1007/s11082-019-1797-9.
- [32] R. Qindeel, Effect of gamma radiation on morphological & optical properties of ZnO nanopowder, *Results Phys.* 7 (2017) 807–809. doi:10.1016/j.rinp.2017.02.003.
- [33] S. Kaya, E. Yilmaz, Modifications of structural, chemical, and electrical characteristics of Er₂O₃/Si interface under Co-60 gamma irradiation, *Nucl. Inst. Methods Phys. Res. B.* 418 (2018) 74–79. doi:10.1016/j.nimb.2018.01.010.
- [34] F. Adrovic, Gamma Radiation, *JanezaTrdine*. 9 (2012) 51000. doi:10.1016/j.mssp.2020.105172.
- [35] B. Oryema, E. Jurua, I.G. Madiba, M. Nkosi, J. Sackey, M. Maaza, Effects of low-dose γ -

- irradiation on the structural , morphological, and optical properties of fluorine-doped tin oxide thin films, *Radiat. Phys. Chem.* 176 (2020) 109077. doi:10.1016/j.radphyschem.2020.109077.
- [36] Y.S. Rammah, A.S. Abouhaswa, A.H. Salama, R. El-Mallawany, Optical, magnetic characterization, and gamma-ray interactions for borate glasses using XCOM program, *J. Theor. Appl. Phys.* 13 (2019) 155–164. doi:10.1007/s40094-019-0331-6.
- [37] O. Agar, H.O. Tekin, M.I. Sayyed, M.E. Korkmaz, O. Culfa, C. Ertugay, Experimental investigation of photon attenuation behaviors for concretes including natural perlite mineral, *Results Phys.* 12 (2019) 237–243. doi:10.1016/j.rinp.2018.11.053.
- [38] G.G. Flores-Rojas, F. López-Saucedo, E. Bucio, Gamma-irradiation applied in the synthesis of metallic and organic nanoparticles: A short review, *Radiat. Phys. Chem.* 169 (2020) 107962. doi:10.1016/j.radphyschem.2018.08.011.
- [39] V. Venkatachalam, R. Jayavel, Novel synthesis of Ni-ferrite (NiFe₂O₄) electrode material for supercapacitor applications, *AIP Conf. Proc.* 1665 (2015) 140016. doi:10.1063/1.4918225.
- [40] D.M. Hemed, Effect of Gamma Irradiation on the Structure Diffusion Coefficient of Co-Zn Doped Ferrite, *Am. J. Appl. Sci.* 2 (2005) 989–992.
- [41] M.A. Ahmed, E. Ateia, G. Abdelatif, F.M. Salem, Charge transfer behavior of erbium substituted Mg–Ti ferrites, *Mater. Chem. Phys.* 81 (2003) 63–77. doi:10.1016/S0254-0584(03)00143-3.
- [42] H. Salazar-Tamayo, K.E.G. Telleza, C.A.B. Meneses, Cation Vacancies in NiFe₂O₄ During Heat Treatments at High Temperatures: Structural, Morphological and Magnetic Characterization, *Mater. Res.* 22 (2019) e20190298. doi:10.1155/IJP/2006/90809.
- [43] M. Kurian, C. Kunjachan, Investigation of size dependency on lattice strain of nanoceria particles synthesised by wet chemical methods, *Int. Nano Lett.* 4 (2014) 73–80. doi:10.1007/s40089-014-0122-7.

- [44] T.C. Paul, M.H. Babu, J. Podder, B.C. Dev, S.K. Sen, S. Islam, Influence of Fe³⁺ ions doping on TiO₂ thin films : Defect generation , d-d transition and band gap tuning for optoelectronic device applications, *Phys. B Phys. Condens. Matter.* 604 (2021) 412618.
doi:10.1016/j.physb.2020.412618.
- [45] S.K. Sen, T.C. Paul, M.S. Manir, S. Dutta, M.N. Hossain, J. Podder, Effect of Fe-doping and post annealing temperature on the structural and optical properties of - MoO₃ nanosheets, *J. Mater. Sci. Mater. Electron.* 30 (2019) 14355–14367. doi:10.1007/s10854-019-01805-z.
- [46] I.M. Hamada, X-ray diffraction and IR absorption in the system Co_{0.6}Zn_{0.4}Mn_xFe_{2-x}O₄ before and after γ -irradiation, *J. Magn. Magn. Mater.* 271 (2004) 318–325.
doi:10.1016/j.jmmm.2003.09.049.
- [47] M. Abhishek, E. Melagiriappa, M. Irfan, M. Veena, B.M. Sahanashree, B.N. Anandaram, H.M. Somashekarappa, Biscoumarin derivative for designing the WLED display applications
Biscoumarin Derivative for Designing the WLED Display Applications, *AIP Conf. Proc.* 2115 (2019) 03015.
- [48] D.S. Nikam, S. V Jadhav, V.M. Khot, R.A. Bohara, C.K. Hong, S.S. Malib, S.H. Pawar, Cation distribution, structural, morphological and magnetic properties of Co_{1-x}Zn_xFe₂O₄ (x= 0–1) nanoparticles Dipali, *RSC Adv.* 5 (2015) 2338–2345. doi:10.1039/C4RA08342C.
- [49] H.M. Zaki, Structure, analysis and some magnetic properties for low temperature fired Ni Cu ferrite, *Phys. B Phys. Condens. Matter.* 407 (2012) 2025–2031. doi:10.1016/j.physb.2012.01.134.
- [50] H.L. Andersen, M. Saura-Múzquiz, C. Granados-Miralles, E. Canévet, N. Locke, M. Christensen, Crystalline and magnetic structure-property relationship in spinel ferrite nanoparticles, *Nanoscale.* 10 (2018) 14902–14914. doi:10.1039/C8NR01534A.
- [51] S.M. Patange, S.E. Shirsath, G.S. Jangam, K.S. Lohar, S.S. Jadhav, S.M. Patange, S.E. Shirsath,

- G.S. Jangam, K.S. Lohar, S.S. Jadhav, Rietveld structure refinement, cation distribution and magnetic properties of Al³⁺ substituted NiFe₂O₄ nanoparticles, *J. Appl.* 109 (2011) 053909. doi:10.1063/1.3559266.
- [52] S.K. Sen, M.S. Manir, S. Dutta, M.H. Ali, M.N.I. Khan, M.A. Matin, M.A. Hakim, Influence of total absorbed dose of Co-60 γ -radiation on the properties of h-MoO₃ thin films, *Thin Solid Films*. 693 (2019) 137700. doi:10.1016/j.tsf.2019.137700.
- [53] K.B. Sapnar, V.N. Bhoraskar, S.D. Dhole, Effects of 6 Mev electron irradiation on ZnO nanoparticles synthesized by microwave method, *Proc. 2011 Part. Accel. Conf. New York, NY, USA.* (2011) 2166–2168.
- [54] A. Reyhani, A. Gholizadeh, V. vahedi, M.R. Khanlari, Effect of gamma radiation on the optical and structural properties of ZnO nanowires with various diameters, *Opt. Mater. (Amst)*. 75 (2018) 236–242. doi:10.1016/j.optmat.2017.10.027.
- [55] P.A. Arasu, R.V. Williams, The dielectric studies on sol – gel routed molybdenum oxide thin film, *J. Adv. Dielectr.* 7 (2017) 1–7. doi:10.1142/S2010135X17500114.
- [56] D.D. Andhare, S.R. Patade, J.S. Kounsalye, K.M. Jadhav, Effect of Zn doping on structural, magnetic and optical properties of cobalt ferrite nanoparticles synthesized via . Co-precipitation method, *Phys. B Phys. Condens. Matter.* 583 (2020) 412051. doi:10.1016/j.physb.2020.412051.
- [57] P. Samoila, C. Cojocaru, I. Cretescu, C.D. Stan, V. Nica, L. Sacarescu, V. Harabagiu, Nanosized Spinel Ferrites Synthesized by Sol-Gel Autocombustion for Optimized Removal of Azo Dye from Aqueous Solution, *J. Nanomater.* 2015 (2015) 713802.
- [58] P.Y. Reyes-rodríguez, D.A. Cortés-hernández, J.C. Escobedo-bocardo, J.M. Almanza-robles, H.J. Sánchez-fuentes, L.E. De León-prado, J. Méndez-nonell, G.F. Hurtado-lópez, Structural and magnetic properties of Mg-Zn ferrites (Mg_{1-x}Zn_xFe₂O₄) prepared by sol-gel method, *J. Magn.*

- Magn. Mater. 427 (2017) 268–271. doi:10.1016/j.jmmm.2016.10.078.
- [59] H. Berhanu, A.T. Raghavender, L. Kebede, T. Anjaneyulu, Ferromagnetic Behavior in Zinc Ferrite Nanoparticles Synthesized using Coprecipitation Technique, *Sci. Technol. Arts Res. J.* 3 (2014) 85–88.
- [60] K.M. Badoo, M.S. Ansari, Low temperature-fired Ni-Cu-Zn ferrite nanoparticles through autocombustion method for multilayer chip inductor applications, *Nanoscale Res. Lett.* 7 (2012) 1–14. doi:10.1186/1556-276X-7-112.
- [61] M.G. Naseri, E.B. Saion, M. Hashima, A.H. Shaari, H.A. Ahangar, Synthesis and characterization of zinc ferrite nanoparticles by a thermal treatment method, *Solid State Commun.* 151 (2011) 1031–1035. doi:10.1016/j.ssc.2011.04.018.
- [62] S. Asiri, M. Sertkol, H. Güngüneş, M. Amir, A. Manikandan, I. Ercan, A. Baykal, The Temperature Effect on Magnetic Properties of NiFe₂O₄ Nanoparticles, *J. Inorg. Organomet. Polym. Mater.* 28 (2018) 1587–1597. doi:10.1007/s10904-018-0813-z.
- [63] B. Sarkar, B. Dalal, V. Dev Ashok, K. Chakrabarti, A. Mitra, S.K. De, Magnetic properties of mixed spinel BaTiO₃-NiFe₂O₄ composites, *J. Appl. Phys.* 115 (2014) 123908. doi:10.1063/1.4869782.
- [64] M.S. Hossain, S.M. Hoque, S.I. Liba, S. Choudhury, Effect of synthesis methods and a comparative study of structural and magnetic properties of zinc ferrite, *AIP Adv.* 7 (2017) 105321. doi:10.1063/1.5009925.
- [65] S.K. Sharma, R. Kumar, V. V. Siva Kumar, M. Knobel, V.R. Reddy, A. Gupta, M. Singh, Role of electronic energy loss on the magnetic properties of Mg_{0.95}Mn_{0.05}Fe₂O₄ nanoparticles, *Nucl. Instruments Methods Phys. Res. Sect. B Beam Interact. with Mater. Atoms.* 248 (2006) 37–41. doi:10.1016/j.nimb.2006.03.188.

- [66] A. Karim, S.E. Shirsath, S.J. Shukla, K.M. Jadhav, Gamma irradiation induced damage creation on the cation distribution, structural and magnetic properties in Ni-Zn ferrite, *Nucl. Instruments Methods Phys. Res. Sect. B Beam Interact. with Mater. Atoms.* 268 (2010) 2706–2711. doi:10.1016/j.nimb.2010.05.058.
- [67] R.S. Yadav, I. Kuřitka, J. Vilcakova, J. Havlica, J. Masilko, L. Kalina, J. Tkacz, J. Švec, V. Enev, M. Hajdúchová, Impact of grain size and structural changes on magnetic, dielectric, electrical, impedance and modulus spectroscopic characteristics of CoFe₂O₄ nanoparticles synthesized by honey mediated sol-gel combustion method, *Adv. Nat. Sci. Nanosci. Nanotechnol.* 8 (2017) 045002. doi:10.1088/2043-6254/aa853a.
- [68] B. Parvatheeswara Rao, K.H. Rao, P.S.V. Subba Rao, A. Mahesh Kumar, Y.L.N. Murthy, K. Asokan, V. V. Siva Kumar, R. Kumar, N.S. Gajbhiye, O.F. Caltun, Swift heavy ions irradiation studies on some ferrite nanoparticles, *Nucl. Instruments Methods Phys. Res. Sect. B Beam Interact. with Mater. Atoms.* 244 (2006) 27–30. doi:10.1016/j.nimb.2005.11.009.